Analysis of Multilayered Power Module Packaging Behavior Under Random Vibrations

Di Liang, Qiong Wu, Davood Ghaderi, and Josep M. Guerrero, *Fellow, IEEE*

***Abstract*— Solder joints are the critical components of the printed circuit boards (PCBs) in the moving electronic systems, such as satellites and automotive industries that are most vulnerable to accidental vibrations. Therefore, the reliability of these boards since they are designed to be used for long-time applications is important. Since the laboratory tests are time-consuming and require well-equipped and costly measurement devices, reliability tests are preferred to perform through the analytical methods. In this article, an analytical model based on the multilayer plate theory is presented for the random vibration analysis, and the results are obtained for the different vibration frequencies, including the natural vibration frequency. For the proposed model, the state of the PCB layer and the amount of the stress in the solder joints are investigated separately, and the normal and shear stresses are obtained through the combined sinusoidal–exponential equation. Results by the finite-element method (FEM) analysis show that the cracks form at the edge of the interconnection points of the board, and the solder and void formation and crack propagation appear in the corners of the PCB in frequencies closed to the natural vibration frequency. Reliability increases by the reduced solder height.**

***Index Terms*— Fatigue life, solder, vibration.**

I. Introduction

PRINTED circuit boards (PCBs) are subjected to be applied in moving systems, such as the automotive, airplane and satellite industries, communication systems, intermediate blocks for the load and renewable energy sources (RESs), and low and high power utilization in electrical and electronics industries. Therefore, the reliability of these boards is important based on the demand for the long-term applications of the PCBs. For example, PCBs, in automotive, should be designed to work for at least 15 years with high reliability [1], [2].

Manuscript received May 9, 2020; accepted May 16, 2020. Date of publication May 19, 2020; date of current version October 5, 2020. This work was supported by VILLUM FONDEN [Center for Research on Microgrids (CROM)] under the VILLUM Investigator Grant 25920. Recommended for publication by Associate Editor C. Basaran upon evaluation of reviewers' comments. *(Corresponding authors: Di Liang; Davood Ghaderi.)*

Di Liang is with the College of Mechanical Engineering, Saitama Institute of Technology, Saitama 369-0293, Japan (e-mail: ilangdi@163.com).

Qiong Wu is with the College of Mechatronic Engineering, Nanjing Forestry University, Nanjing 210037, China (e-mail: wqiong@163.com).

Davood Ghaderi is with the Electrical and Electronics Engineering Department, Bursa Technical University, 16310 Bursa, Turkey (e-mail: davood.ghaderi@btu.edu.tr).

Josep M. Guerrero is with the Center for Research on Microgrids (CROM), Department of Energy Technology, Aalborg University, 9220 Aalborg, Denmark (e-mail: joz@et.aau.dk).

Color versions of one or more of the figures in this article are available online at http://ieeexplore.ieee.org.

Digital Object Identifier 10.1109/TCPMT.2020.2995735

Thermal and vibration loading are the most important parameters that can affect the long-life of these boards. Solder joints are the interconnection points between the electronic components and the PCB, and the electrical and physical active ingredients such as vibration influence these adhesion points. Especially when a PCB is inserted into a moving system such as the airplane or the satellite, the effect of the parameters such as vibration should be considered on the solder joints. Laboratory tests are time-consuming and need costly equipment to test and measure the effects of these parameters on the fatigue of a PCB.

Therefore, analytical models are preferred to assess these effects. There are studies to present the impact of thermal loading and tension in solder joints under random vibrations. A demolition mechanism based on the theory of the viscoplasticity model is presented in [3] and [4] for investigation of the behavior of the Pb40/Sn60 solder alloy. Since the equations of the solder damage are considered in the proposed constitutive model, both the fatigue and stress analyses can be done simultaneously. These studies consider the thermal loading effects on the fatigue of the surface-mount packaging (SMP).

Basaran and Chandaroy [5] proposed a nonlinear and time-domain-based analysis model to obtain the lifetime of the SMP under a unified vibration mechanism. This study shows that for material in the elastic range, higher damage will be experienced for the higher vibration frequencies. However, for the inelastic range, low loading frequencies can harm more the solders in the per cycle. Furthermore, a model for combined thermal cycling and dynamic vibration loading effect on the SMP is presented in [6] that uses the superposition rules and obtains the fatigue life of the solders separately for these effects. This article shows that the vibration and thermal strains have elastic and inelastic behaviors on the solder interconnections and should be considered simultaneously for fatigue investigation of the SMP especially for the moving systems, such as the automotive and military applications.

Moiré interferometry (MI) is used for the solder joints of the ball grid array (BGA) to obtain the fatigue of the solders under both thermal and dynamic vibration loadings in [7]. The main outcome of this article is that it proves the dynamic vibrations can evoke the inelastic strains on the BGA with low melting point and high viscoplasticity specifications, while the general belief was that vibration with strains has the elastic behavior. The results of [8] confirm the theory of "smaller is stronger" for micrometer-scale material analysis through the MI model to measure the cyclic inelastic in-plane corruption. The study shows that MI is not accurate enough for

simultaneous environment analysis because it does not include and consider the scale effect and the thermal and dynamic interaction.

Miner's rule has been considered in [9] to investigate the accumulative harm of the thermal and vibration loadings separately. The study shows that the SMP has a shorter long-life under both vibration and thermomechanical effects. Despite that the effect of the dynamic loading is not considered on the fatigue life of the package, this study illustrates that for an accurate estimation for the fatigue life of the SMA, the vibration has to be considered. An analytic-mode-based isothermal test by considering the MI model has been done for the multilayered orthotropic-laminated thin baseplate in [10]. The research work investigates the peeling and shear stresses for the layers on the thin substrate under the thermal gradient. This study shows that the proposed analytical model gives more noticeable and accurate results in comparison with software results. Although for the isothermal loading consideration in the packaging, designers consider an average temperate by considering the temperature of the top and bottom of the package. In this sense, Basaran and Wen [11] presented an accurate model to estimate the temperature of any place of the microelectronic package based on a thermal gradient analysis. According to this study results, for the laminated solder layer, considering the isothermal temperature as the thermal loading decreases, the accuracy of the calculations and shear and peeling stresses cannot be estimated correctly.

A simple analytical model is presented in [12] for orthotropic structures with considering the thermal impact of the interface compatibility layers. This study shows that the softer epoxy for the solder layer can decrease the shear and axial normal stresses for the affiliated layer that can directly decrease the die crack propagation. Lee and Basaran [13] presented a review study and compared nine creep models to investigate the accuracy of them under thermal cycling loadings and the same test data. The creep strain rate is modeled by sinusoidal, exponential, and sinusoidal–exponential equations through the proposed models. The results of this study show that for the creep stress prediction, the sinusoidal–exponential models are more accurate. Also, models that consider only the shear stress are not efficient. For the stress calculations, grain size should be considered, and models that do not consider this effect are not accurate. The finite-element method (FEM) has been considered for all of these studies to evaluate the nonlinear dynamic analysis for microelectronic devices.

In the abovementioned studies, the thermal loading effects were focused and dynamic vibrations were placed against the background of the temperature analysis generally and only the vibration analysis has not been done in these works separately. Indeed, some of the studies have focused on the vibration loading effect of the fatigue life of the solder layers. For example, in [14], the crack formation and propagation is analyzed and it is concluded that the corner points of the PCB are the most affected areas and solders at the corners are exposed to damage under the random dynamic loadings. Xia *et al.* [15] and Meng and Dasgupta [16] show that the angle of the vibration is important and shearing stress for microelectronic packaging is the most for the electronic

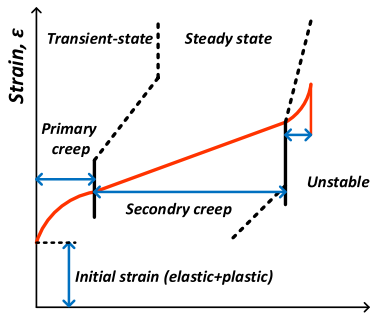

Fig. 1. Creep stages under constant load.

boards placed perpendicular to the surface that experiences the greatest amount of the stress at the soldered points. The work in [17] and [18] compares the different materials for the solders and concludes that the SAC387 experiences the maximum amount of the peeling stress for the microelectronic packaging under the dynamic loadings.

In [19] and [20], the electronic board is assumed with two layers and the spatial variations are obtained based on the point analysis. Therefore, the strain value of each solder joint is obtained. As a result, by applying Hook's law, the stress of each solder joint under flexural moment loading is calculated. This model is also used only to obtain the normal stresses so that shear and bending stresses cannot be obtained.

In this article, based on the multilayer shell theory, the PCB is considered as a 2-D plate and a sinusoidal–exponential analytical model is presented to obtain the fatigue life and the amount of the stress in the solder joints under the random vibration. In addition, the damage to solder joints in these sensitive structures will be investigated using fracture mechanics models. Results show that the corners of the PCB are most exposed to the stress and crack formation and void propagation density are higher at these locations.

II. Improved Multilayer Shell Theory

Creep strain easily is demonstrated by holding the material under constant stress for the long periods of the time and observing the ensuing deformation increasing over time. There are three observable phases for the creep shown in Fig. 1.

The initial portion or the first phase is called the "transient phase" as shown in Fig. 1 is consistent with the proportional stress–strain relationship. This is followed by the nonlinear phase where the strain rate seems to decrease with respect to time. This is the stage where the solder matrix undergoes the stress relaxation, and hence, the proportional relationship between the stress and strain is lost.

The second stage is called the "steady-state" phase. In this phase, the flow stress required to maintain the plastic deformation of the solder matrix is more or less constant. Therefore, one sees a constant strain rate with respect to the time. The second phase is followed by the third stage labeled as "unstable" in this figure. This is the stage where the strain rate required to maintain is no longer constant and the solder begins to experience the damage due to the creep. Solder is

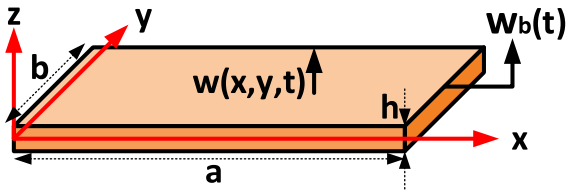

Fig. 2. Thin rectangular plate.

a high surface energy material and is, therefore, inherently unstable.

Upon being subjected to the thermal cycling and aided by the mechanical stresses or a combination thereof, the material absorbs the incoming energy directed toward the solder joint system and returns to the equilibrium state of the low surface energy.

This process takes place through the gradual phase and grain coarsening that weakens the solder joint structure due to a reduction in net surface area of contact, consequently, making it susceptible to failure in areas of high-stress concentration. To evaluate the tensions and stresses on the solder joint in the microelectronic package, at the first step, the PCB should be modeled. For this purpose, based on the multilayer shell theory, the isotropic plate is considered. A thin rectangular isotropic plate is shown in Fig. 2, and the vibration equation for that is written as follows [21]:

$$\rho\frac{\partial^2 w}{\partial t^2}+c\frac{\partial w}{\partial t}+D\nabla^4 w=0 \tag{1}$$

where ρ and c, respectively, are the density and the damping coefficient of the sheet relative to the surface unit and D is the flexural stiffness of the sheet. Sheet displacement is given by the following equation:

$$w_a(x,y,t)=w_b(t)+w(x,y,t) \tag{2}$$

where w_a and w_b are the absolute and boundary displacements, respectively, and w is the displacement relative to the boundary. Relation (3) results from the substitution of (2) in (1)

$$\rho\frac{\partial^2 w}{\partial t^2}+c\frac{\partial w}{\partial t}+D\nabla^4 w=p(t). \tag{3}$$

Equation (3) can be solved by the following equation:

$$w(x,y,t)=\sum_{m=1}^{\infty}\sum_{n=1}^{\infty}\psi_{mn}(x,y)q_{mn}(t). \tag{4}$$

The shapes of the modes considered are perpendicular to each other. The eigenfunction for the mnth and klth mode are considered by the $\psi_{mn}(x,y)$ and $\psi_{kl}(x,y)$, while $q_{mn}(t)$ is the time-varying function.

By replacing (4) into (3) and if the two sides of this relation are multiplied by $\psi_{kl}(x,y)$, the integral is obtained from the area of the sheet R

$$\ddot{q}_{mn}(t)+\beta_{mn}\dot{q}_{mn}(t)+\omega_{mn}q_{mn}(t)=\frac{1}{m_{mn}}\int\psi_{mn}(x,y)p(t)dxdy. \tag{5}$$

In (5), ω_{mn} and β_{mn}, respectively, are the undamped natural frequency and the frequency bandwidth for the mnth mode of the plate. β_{mn} can be presented as

$$\beta_{mn}=\frac{c_{mn}}{m_{mn}}=2\xi_{mn}\omega_{mn}\ \text{and}\ c_{mn}=\frac{c}{\rho}m_{mn}. \tag{6}$$

In (6), the damping ratio of the mnth mode is shown with ξ_{mn}. c_{mn} and m_{mn} are the model damping and model mass, respectively.

Now, if the base of the sheet is induced with the harmonic function $w_b(t)=e^{-i\omega t}$, the value of $p(t)$ is written as follows:

$$w_b(t)=e^{-i\omega t},\quad p(t)=-\rho\ddot{w}_b(t)\rightarrow p(t)=\rho\omega^2e^{-i\omega t}. \tag{7}$$

By inserting (7) into (5), (5) can be written in the form of the following equations:

$$\ddot{q}_{mn}(t)+\beta_{mn}\dot{q}_{mn}(t)+\omega^2q_{mn}(t)=\frac{\rho\omega^2I_{mn}}{m_{mn}}e^{-i\omega t} \tag{8}$$

$$I_{mn}=\int\psi_{mn}(x,y)dxdy. \tag{9}$$

By solving (8), q can be obtained by the following equations:

$$q_{mn}(t)=H_{mn}(\omega)I_{mn}e^{-i\omega t} \tag{10}$$

$$H_{mn}(\omega)=\frac{\rho\omega^2}{m_{mn}\left(-\omega^2+\beta_{mn}i\omega+\omega_{mn}^2\right)}. \tag{11}$$

By substituting (10) into (4), the frequency response of the sheet vibration displacement is obtained as follows:

$$H_w(x,y,\omega)=\sum_{m=1}^{\infty}\sum_{n=1}^{\infty}\psi_{mn}(x,y)H_{mn}(\omega)I_{mn}. \tag{12}$$

Then, since the system response is equal to the result of multiplying the system input by the frequency response function, the frequency response function of an isotropic sheet is obtained as follows:

$$H_{wa}(x,y,\omega)=1+H_w(x,y,\omega). \tag{13}$$

The frequency response function was obtained using the input of the harmonic function, but since the frequency response function depends on the physical properties of the plate, it can also be used for random input loads. Using random vibration equations, the standard deviation $E[w^2(x,y)]$ and acceleration $E[\ddot{w}_a^2(x,y)]$ values at each point of the plate are obtained as (14) and (15) with one-sided power spectrum density (PSD) of $S_{w_b}(\omega)$

$$E\left[w^2(x,y)\right]=\int_0^{\infty}|H_w(x,y,\omega)|^2S_{w_b}(\omega)d\omega \tag{14}$$

$$E\left[\ddot{w}_a^2(x,y)\right]=\int_0^{\infty}\omega^4|H_w(x,y,\omega)|^2S_{w_b}(\omega)d\omega. \tag{15}$$

Using the preceding equations, the standard deviation of the displacement and the acceleration of the sheet are obtained at each point. In fact, the sheet curves as a standard deviation. However, the amount of stress resulting from this curvature is obtained in solder joints.

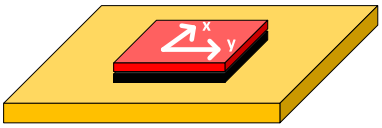

Fig. 3. Simple state for the continuous interface layer to model the solder joint interconnection to the plate.

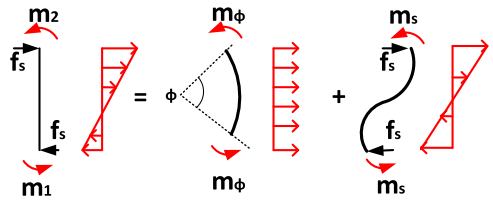

Fig. 4. Moments under the continuous interconnect layer [21].

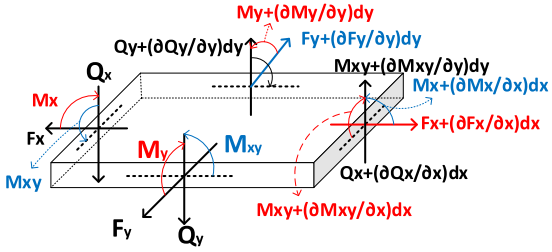

Fig. 5. PCB modeling by considering the vibration effects on the plate.

III. Solder Joints

For the PCB, the number of the solder joints is considered to be numerous so that the interface layer can be continuously assumed and multilayer sheet theory is used to model this problem. Fig. 3 is considered for the interconnection layer of the solder and plate.

The free-body diagram of the board and the interface layer are considered, as shown in Figs. 4 and 5, respectively. Assuming that the normal and shear stress values are constant over the solder thickness, while the amount of linear bending moment varies with the edge of the electronic board equal to m_2 and on the edge of the electronic part equal to m_1, the value of r is constant and is defined as (16) and (17) [22]–[25]. m_1 and m_2 can be presented as follows:

$$m_{2x} = r_x m_{1x} \tag{16}$$

$$m_{2y} = r_x m_{1y} \tag{17}$$

where r_x and r_y are two coefficients that depend on the normal and shear deformations.

In Fig. 4, the amount of moment along the solder is shown. The moment at each joint can be divided into m_φ in the beam, which makes the simple bending and is constant during the solder length, and the torque m_s, which also cuts during the solder length, and generates a linear along the solder length as follows:

$$m_{\varphi x} = \frac{m_{2x} - m_{1x}}{2} \text{ and } m_{\varphi y} = \frac{m_{2y} - m_{1y}}{2} \tag{18}$$

$$m_{sx} = \frac{m_{2x} + m_{1x}}{2} \text{ and } m_{sy} = \frac{m_{2y} + m_{1y}}{2}. \tag{19}$$

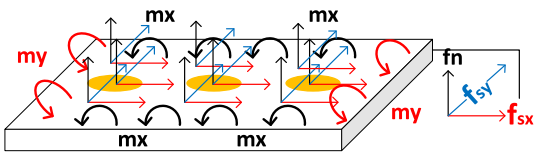

Fig. 6. Interconnection of solder joints and the plate and the state of the PCB under vibration.

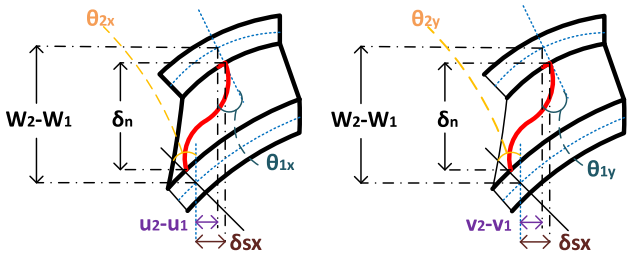

Fig. 7. Simple model for the isotropic sheet.

Also, the relationship between normal stress $f_n(x)$, shear stress $f_s(x)$, and moment $m_\varphi(x)$ can be written as relationships (20)–(22). In these equations, the equivalent hardness values can be obtained for the interface layer in the form of the coefficients k_n, k_s, and k_φ

$$f_n(x) = k_n \times \delta_n(x) \text{ and } k_n = \frac{nE_3A_s}{h_3} \tag{20}$$

$$f_s(x) = k_s \times \delta_s(x) \text{ and } k_s = \frac{nG_3A_s}{h_3} \tag{21}$$

$$m_\varphi(x) = k_\phi \times \phi(x) \text{ and } k_\varphi = \frac{nE_3I_s}{h_3}. \tag{22}$$

In these equations, $\delta_n(x)$, $\delta_s(x)$, and $\phi(x)$ present the transverse normal, shear, and angular deformations, respectively. n is the number of the solder joints and A_s and I_s are the solder cross-sectional area and the moment solder surface, respectively. h_3, E_3, and G_3 present the height, shear, and elastic modulus for the material of the solders. Now, by considering Figs. 5 and 6, by writing the moment equilibrium around the y-axis, the moment equilibrium around the y-axis and the equilibrium force along the z-axis can be obtained.

For the plate, the relationships between the moment and the bending sheet are in the form of the following equations:

$$m_x + \int m_{1x}dx = D_i\left(\frac{\partial^2 w}{\partial x^2} + \upsilon\frac{\partial^2 w}{\partial y^2}\right) \tag{23}$$

$$m_y + \int m_{1y}dy = D_i\left(\frac{\partial^2 w}{\partial y^2} + \upsilon\frac{\partial^2 w}{\partial x^2}\right) \tag{24}$$

$$m_{xy} = D_i(\upsilon - 1)\frac{\partial^2 \mathrm{w}}{\partial x \partial y}. \tag{25}$$

In the recent equations, D_i and υ are the flexural rigidity and vibration frequency, respectively. By writing the moment equilibrium in the interface layer, relationships (26) and (27) will be obtained

$$f_{sx} = \frac{m_{2x} + m_{1x}}{h_3} = \frac{2m_{sx}}{h_3} \tag{26}$$

$$f_{sy} = \frac{m_{2y} + m_{1y}}{h_3} = \frac{2m_{sy}}{h_3}. \tag{27}$$

The governing normal stress equation can be obtained in the form of the following equation [22]:

$$\frac{\partial^4 f_n}{\partial x^4} + 2\frac{\partial^4 f_n}{\partial x^2 \partial y^2} + \frac{\partial^4 f_n}{\partial y^4} - A\frac{\partial^2 f_n}{\partial x^2} - B\frac{\partial^2 f_n}{\partial y^2} - Cf_n = 0. \tag{28}$$

$A - D$ are coefficients that are depended on r_x, equivalent hardness values for the interface layer k_n and k_ϕ, and height of the solder and plate interconnection points h_1 and h_2. The sum of the normal stresses in solder joints with the inertia force resulting from the acceleration of the electronic component is equal to the following equation:

$$\int_{-L}^{L}\int_{-T}^{T} f_n dx dy = m_{ic}\alpha \tag{29}$$

where L and T are half of the length and width of the electronic component at the solder interconnection, respectively. m_{ic} and α are the moment along with the interface point and characteristic constant of the normal deformation. The slope in the vertical and horizontal symmetrical axes is equal to zero:

$$\frac{\partial \delta_n}{\partial x}(x,0) = 0, \quad \frac{\partial f_n}{\partial x}(x,0) = 0 \tag{30}$$

$$\frac{\partial \delta_n}{\partial y}(y,0) = 0, \quad \frac{\partial f_n}{\partial y}(y,0) = 0. \tag{31}$$

The difference between the curvature of the board and the component is equal to the following equations:

$$\frac{\partial^2 \delta_n}{\partial x^2} = \frac{1}{R_{x\text{PCB}}} - \frac{1}{R_{x\text{IC}}} \rightarrow \frac{\partial^2 \delta_n}{\partial x^2} = \frac{1}{R_{xPCB}} \xrightarrow{\times k_n} \frac{\partial^2 f_n}{\partial x^2} = \frac{k_n}{\text{RMS}(R_{x\text{PBC}})} \tag{32}$$

$$\frac{\partial^2 f_n}{\partial y^2} = \frac{k_n}{\text{RMS}\left(R_{y\text{PBC}}\right)} \tag{33}$$

where $R_{x\text{PBC}}$ and $R_{y\text{PBC}}$ are the normal stress around the x and y-axes. To solve the abovementioned relationship, the method of repeated changes is used. Due to the stress changes in the joints, the initial response of this function is chosen as follows:

$$f_0 = a + be^{cx} + de^{fy}. \tag{34}$$

The relationship between the displacement and the moment is nonlinear, so the system input is chosen as a parameter that has a linear relationship with the moment. Since the moment is linearly related to the curvature (*1/R*), it can also be written for their standard deviation. The values of the normal stress and the bending moment stress at each solder joint are obtained by (35) and (38)

$$\text{RMS } R_{x\text{PCB}} = \iint m_x dx dy \tag{35}$$

$$\text{RMS } R_{y\text{PCB}} = \iint m_y dx dy \tag{36}$$

$$\text{RMS } M = \sqrt[2]{\text{RMS } m_x^2 + \text{RMS } m_y^2} \tag{37}$$

$$\text{RMS } \sigma_b = \frac{\text{RMS } M \times p}{I} \tag{38}$$

where p is equal to the solder radius and I is the second inertial moment of the surface around the neutral axis. The area of the high integrals is the location of each connection relative to the center of the electronic component.

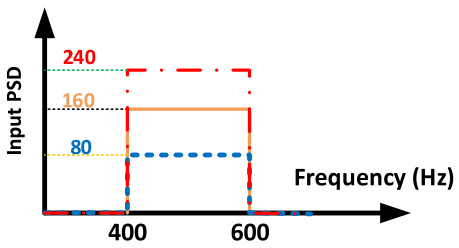

Fig. 8. Input PSD.

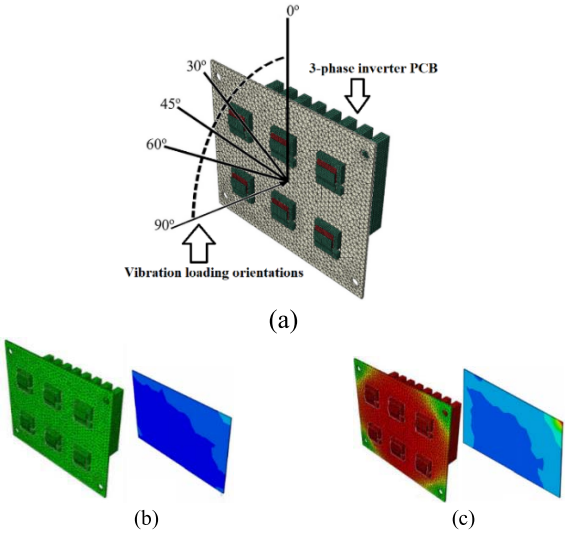

Fig. 9. State of the PCB under random vibration loading with (a) 90° and (b) 0° orientations.

IV. Reliability Validation With Finite-Element Model

In random vibration analysis, it is assumed that the loading and response are statistically present in nature and can be represented by a zero-average normal (i.e., Gaussian) distribution. A package with 5.15 × 6.15 mm^2 is considered for PCB, including a power inverter structure with six power MOSFETs and six heatsinks on a PCB. Different values of the PSD, including the 80, 160, and 240 $(\text{m/s}^2)^2$/Hz, are considered according to Fig. 8 to affect the assembly board, and the results will be reported. Based on the mentioned package specifications, around 95 000 nodes and 63 000 elements have been calculated for approving the sensitivity of the board. Fig. 8 shows the input PSD for the selected PCB. Three different PSDs, including 80, 160, and 240 $(\text{m/s}^2)^2$/Hz, and frequencies between 400 and 600 Hz are considered for the vibration test process since the natural frequency of the mentioned board is obtained around 460 Hz by the FEM analysis. Fig. 10 reports the test results for these PSD values.

Resonance is the tendency of the system to oscillate with the maximum amplitude at specific frequencies called resonance

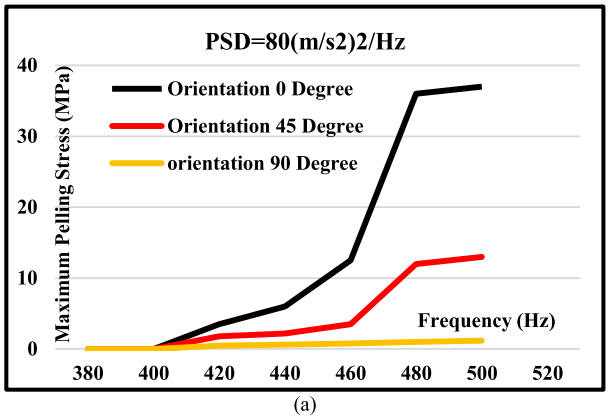

(a)

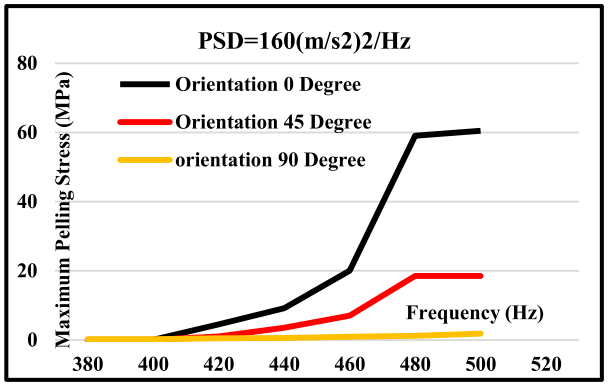

(b)

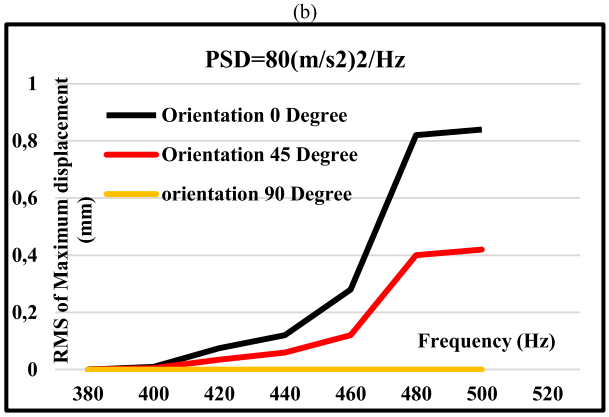

(c)

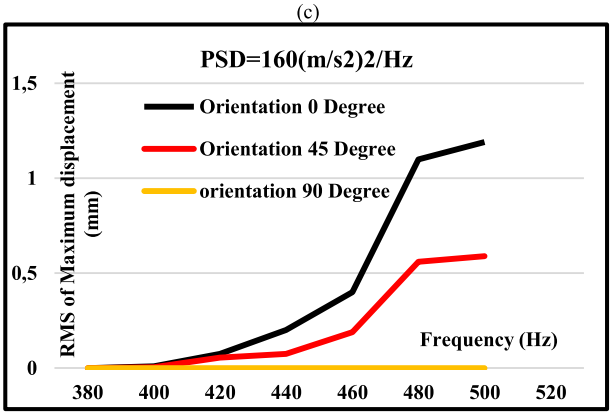

(d)

Fig. 10. RMS values of the maximum peeling stress under (a) 80 and (b) 160 PSD and maximum displacements under (c) 80 and (d) 160 PSD versus frequency.

or natural frequencies. At such frequencies, vibrational energy is stored in the body and, as a result, a small, alternating force can cause a large amplitude oscillatory motion. Fig. 9(a) shows

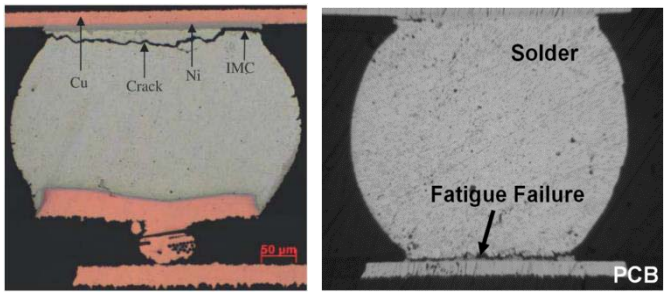

Fig. 11. Simple model for the isotropic sheet [21], [24].

the proposed PCB with power switches and heat sinks and Fig. 9(b) and (c) shows the state of the mentioned board under 90° and 0° of the direction vibration loading. As can be seen from Fig. 9(b), the highest reliability can be obtained under vibration with 90° of the direction.

Another interesting result for the FEM analysis can be seen in Fig. 9(c). As expected, the corners of the PCB board are more affected under higher loading directions and the maximum stress can be obtained in these sections. For our testes, the results of the FEM analysis show that the stress at the corners for 0° as the loading direction is around 20 times greater than the stress value for 90° of the direction. The main outcome of these test results is that the crack formation and propagation are more possible for the corner points for a PCB under 0° of the vibration that is an important parameter for the reliability of the PCB board.

V. Examination of Solder Joint Damage

For the solder joint of the mentioned PSB under various PSDs, the root-mean-square (RMS) values of the peeling stress are presented in Fig. 10. Based on results, for higher values of PSD inputs, higher values for the peeling stresses are reported. Based on this figure, the sample is tested under 0°, 45°, and 90° vibrations. It shows that under 90° vibrations, the minimum values of the stresses are reported.

The interesting result is that the input PSD's higher frequencies effects are neglectable under 90° vibrations, and just the opposite, vibration under 0° can be affected by input frequency and dramatically increased after 460 Hz with a sharp rise. This shows that the optimal design for the components on a PCB can decrease the failure risk. As expected, the stress at the edges is maximal and for the closer to the center of the board will get the lower values. Accurately in the results, the amount of stress due to the acceleration of the electronic component at random vibration is much lower than the stress due to bending. It can be concluded that in this loading, the bending stress has a major contribution to the total stress value of the solder joint. Fig. 11 shows the results of laboratory tests performed by other researchers showing that most cracks extend from the outer edge closer to the electronic board. This confirms that stress is higher near the electronic board. With the PCB vibration, two curvature values for each point of the board can be assumed.

Table I presents the results of the FEM analysis for the mentioned PCB under 0°, 45°, and 90° of the orientations. For

TABLE I
OBTAINED C AND K PARAMETERS

	0°	45°	90°
C(10^{-9})	0.28	2.31	1.74
K	2.28	1.93	1.54

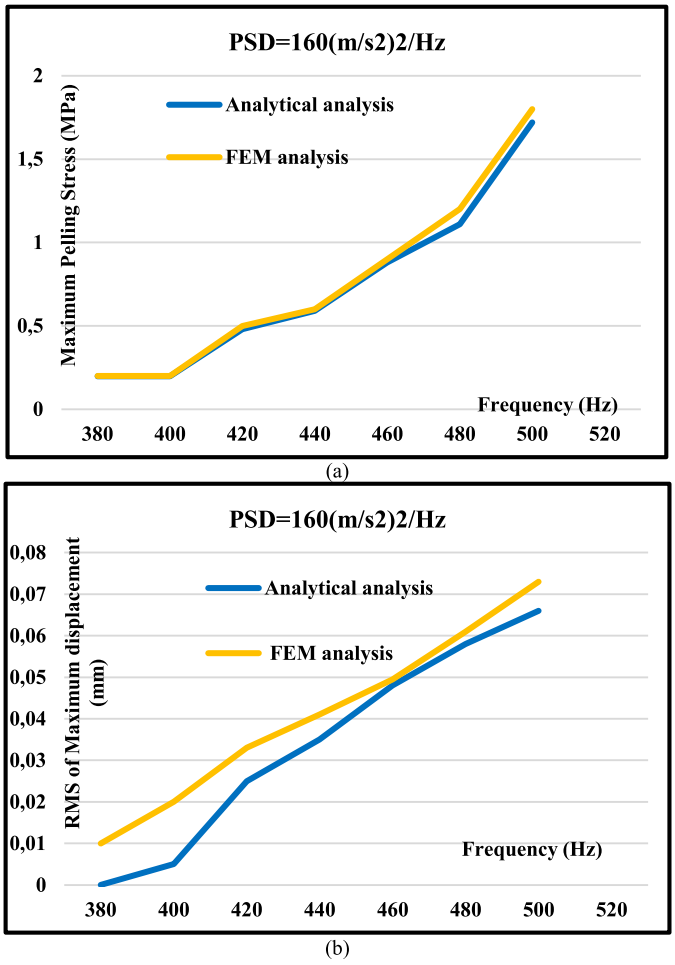

Fig. 12. FEM and the proposed analytical methods comparisons (a) for the maximum peeling stress and (b) maximum displacement under 160 PSD.

obtaining these results, the natural frequency and maximum peeling stresses are considered. In Table I, C and K are two parameters that present the material constants for the solder joints.

If the number of cycles is presented by N_S, the relation between C and K can be presented as follows:

$$S^K N_S = C. \tag{39}$$

Results show that the value of shear stress has a key role in fracture behavior in the solders. This presents that for the lower orientation degrees, the shear stress is increasing and the lifetime of the package dramatically decreases for the lower loadings. Fig. 12(a) and (b) shows the results of the maximum peeling stress and RMS of the maximum displacement at the solder joints for the proposed PCB under 160 $(m/S^2)^2/Hz$ of the input PSD by the FEM and proposed analytical methods. As can be seen, there is a good overlap between two approaches and values are very close to each other.

VI. CONCLUSION

In this article, the stress in the solder joints of a PCB under the random vibration loadings is obtained through an analytical sinusoidal–exponential stress equation. For the fatigue analysis, the theory of the multilayer plate is used as the fundamental generality and the stress–strain and stress behavior of the solder joints are investigated. The study simply models the plate in two dimensions and crack formation and propagation are analyzed according to the optimized equation.

The results of this method show that higher curvature causes higher stresses in the solders. PCB is tested under different levels of the input PSDs and different orientations. Results show that the length and width of the board are the influential parameters in solder's peeling stress and higher displacement in the solder joints is experienced in higher PSDs. Furthermore, FEM was applied to the proposed method. The study shows that the stresses in the solder joints are directly related to the location of the interconnections points in the PCB, the dimension and height of the solder joints, damping of the vibration, the size and elasticity of the electronic component at the connection points, and the density of the PCB. With the higher damping ratio in the PCB, the displacement at the joints will decrease and strengthen the solder joints at the critical points, which can increase the reliability and fatigue life at these interconnection points.

REFERENCES

[1] B. Gadalla, E. Schaltz, and F. Blaabjerg, "A survey on the reliability of power electronics in electro-mobility applications," in *Proc. Int. Aegean Conf. Electr. Mach. Power Electron. (ACEMP), Int. Conf. Optim. Electr. Electron. Equip. (OPTIM) Int. Symp. Adv. Electromech. Motion Syst. (ELECTROMOTION)*, Sep. 2015, pp. 304–310.

[2] R. Enrici Vaion, M. Medda, A. Mancaleoni, G. Mura, A. Pintus, and M. De Tomasi, "Qualification extension of automotive smart power and digital ICs to harsh aerospace mission profiles: Gaps and opportunities," *Microelectron. Rel.*, vols. 76–77, pp. 438–443, Sep. 2017.

[3] C. Basaran and R. Chandaroy, "Nonlinear dynamic analysis of surface mount interconnects: Part I—Theory," *J. Electron. Packag.*, vol. 121, no. 1, pp. 8–11, Mar. 1999.

[4] C. Basaran and R. Chandaroy, "Nonlinear dynamic analysis of surface mount interconnects: Part II—Applications," *J. Electron. Packag.*, vol. 121, no. 1, pp. 12–17, Mar. 1999.

[5] C. Basaran and R. Chandaroy, "Mechanics of Pb40/Sn60 near-eutectic solder alloys subjected to vibrations," *Appl. Math. Model.*, vol. 22, no. 8, pp. 601–627, Aug. 1998.

[6] R. Chandaroy and C. Basaran, "Damage mechanics of surface mount technology solder joints under concurrent thermal and dynamic loading," *J. Electron. Packag.*, vol. 121, no. 2, pp. 61–68, Jun. 1999.

[7] Y. Zhao, C. Basaran, A. Cartwright, and T. Dishongh, "Thermomechanical behavior of micron scale solder joints under dynamic loads," *Mech. Mater.*, vol. 32, no. 3, pp. 161–173, 2000.

[8] C. Basaran, A. Cartwright, and Y. Zhao, "Experimental damage mechanics of microelectronics solder joints under concurrent vibration and thermal loading," *Int. J. Damage Mech.*, vol. 10, no. 2, pp. 153–170, Apr. 2001.

[9] C. Basaran and R. Chandaroy, "Thermomechanical analysis of solder joints under thermal and vibrational loading," *J. Electron. Packag.*, vol. 124, no. 1, pp. 60–66, Mar. 2002.

[10] Y. Wen and C. Basaran, "An analytical model for thermal stress analysis of multi-layered microelectronic packaging," *Mech. Mater.*, vol. 36, no. 4, pp. 369–385, 2004.

[11] C. Basaran and Y. Wen, "Analysis of multilayered microelectronic packaging under thermal gradient loading," *IEEE Trans. Compon., Packag., Manuf. Technol.*, vol. 29, no. 4, pp. 850–855, Dec. 2006.
[12] C. Basaran and Y. Wen, "Influence of interfacial compliance on thermo-mechanical stresses in multilayered microelectronic packaging," *IEEE Trans. Adv. Packag.*, vol. 29, no. 4, pp. 666–673, Nov. 2006.
[13] Y. Lee and C. Basaran, "A creep model for solder alloys," *ASME J. Electron. Packag.*, vol. 133, no. 4, Nov./Dec. 2011, Art. no. 044501, doi: 10.1115/1.4005288.
[14] J. Li, B. Jing, Z. Sheng, F. Lu, X. Jiao, and H. Dai, "GARCH based degradation modeling of solder joint under vibration loading," in *Proc. Prognostics Syst. Health Manage. Conf. (PHM-Harbin)*, Harbin, China, Jul. 2017, pp. 1–5.
[15] J. Xia, G. Li, B. Li, L. Cheng, and B. Zhou, "Fatigue life prediction of package-on-package stacking assembly under random vibration loading," *Microelectron. Rel.*, vol. 71, pp. 111–118, Apr. 2017, doi: 10.1016/j.microrel.2017.03.005.
[16] J. Meng and A. Dasgupta, "MEMS packaging reliability in board-level drop tests under severe shock and impact loading conditions—Part II: Fatigue damage modeling," *IEEE Trans. Compon., Packag., Manuf. Technol.*, vol. 6, no. 11, pp. 1604–1614, Nov. 2016.
[17] J. Xia, L. Cheng, G. Li, and B. Li, "Reliability study of package-on-package stacking assembly under vibration loading," *Microelectron. Rel.*, vol. 78, pp. 285–293, Nov. 2017, doi: 10.1016/j.microrel.2017.09.012.
[18] L. Zhang, C. Huang, W. Huang, T. Li, and J. Hua, "Study of package-on-package solder joints under random vibration load based on Patran," in *Proc. 17th Int. Conf. Electron. Packag. Technol. (ICEPT)*, Wuhan, China, Aug. 2016, pp. 443–447, doi: 10.1109/ICEPT.2016.7583172.
[19] E. Suhir, "On a paradoxical phenomenon related to beams on elastic foundation: Could external compliant leads reduce the strength of a surface-mounted device?" *J. Appl. Mech.*, vol. 55, no. 4, pp. 818–821, Dec. 1988.
[20] M. L. Wu and J. S. Lan, "Investigation and prediction of solder joint failure analysis for ball grid array package subject to mechanical bending environment," *Soldering*, vol. 29, no. 2, pp. 75–84, 2017, doi: 10.1108/SSMT-06-2016-0012.
[21] A. H. Hosseinloo, F. F. Yap, and N. Vahdati, "Analytical random vibration analysis of boundary-excited thin rectangular plates," *Int. J. Struct. Stability Dyn.*, vol. 13, no. 3, Apr. 2013, Art. no. 1250062, doi: 10.1142/s0219455412500629.
[22] E. H. Wong and C. K. Wong, "Approximate solutions for the stresses in the solder joints of a printed circuit board subjected to mechanical bending," *Int. J. Mech. Sci.*, vol. 51, no. 2, pp. 152–158, Feb. 2009.
[23] F. Shirmohamadli, "Analytical investigation of induced stresses on solder joints of electronic boards under random vibration," *Modares Mech. Eng.*, vol. 18, no. 6, pp. 41–48, 2018.
[24] S. Shaw, "Bending of a thin rectangular isotropic micropolar plate," *Int. J. Comput. Methods Eng. Sci. Mech.*, vol. 20, no. 1, pp. 64–71, Jan. 2019.
[25] C.-Y. Huang, Y.-H. Lin, and P.-F. Tsai, "Developing a rework process for underfilled electronics components via integration of TRIZ and cluster analysis," *IEEE Trans. Compon., Packag., Manuf. Technol.*, vol. 5, no. 3, pp. 422–438, Mar. 2015.

Di Liang received the bachelor's degree in engineering from the Guangxi University of Science and Technology, Liuzhou, China, in 2015, and the master's degree in mechanical engineering from the Saitama Institute of Technology, Saitama, Japan, in 2020, where he is currently pursuing the Ph.D. degree in mechanical engineering.

His research fields include new energy vehicles, mechanical structure optimization design, finite-element simulation, and mechanical vibration.

Qiong Wu received the master's degree in engineering from the Jiangsu University of Technology, Zhenjiang, China, in 2013, and the Ph.D. degree in mechanical engineering from the Saitama Institute of Technology, Saitama, Japan, in 2017.

She worked as a Researcher at the Saitama Institute of Technology in 2018. She is currently a Teacher with Nanjing Forestry University, Nanjing, China. Her research fields include vibration test and analysis, and vibration damping technology.

Davood Ghaderi received the Ph.D. degree from Ataturk University, Erzurum, Turkey, in 2017.

He is currently working at the Electrical and Electronics Engineering Department, Bursa Technical University, Bursa, Turkey. His main fields of interests are power electronics and especially dc–dc and dc–ac converters and controllers and material reliability tests for the power converters applicable for renewable energy sources. From 2018 to 2020, he has published 15 SCI/SCIE articles in IEEE, Elsevier, Wiley, and Springer journals in these subjects.

Josep M. Guerrero (Fellow, IEEE) received the B.S. degree in telecommunications engineering, the M.S. degree in electronics engineering, and the Ph.D. degree in power electronics from the Technical University of Catalonia, Barcelona, Spain, in 1997, 2000, and 2003, respectively.

Since 2011, he has been a Full Professor with the Department of Energy Technology, Aalborg University, Aalborg, Denmark, where he is responsible for the Microgrid Research Program. Since 2014, he has been the Chair Professor with Shandong University, Jinan, China. Since 2015, he has been a Distinguished Guest Professor with Hunan University, Changsha, China. Since 2016, he has been a Visiting Professor Fellow with Aston University, Birmingham, U.K., and a Guest Professor with the Nanjing University of Posts and Telecommunications, Nanjing, China. In 2019, he became a Villum Investigator by The Villum Fonden, which supports the Center for Research on Microgrids (CROM) at Aalborg University, being its the Founder and Director. He has published more than 600 journal articles in the fields of microgrids and renewable energy systems, which are cited more than 50 000 times. His research interest is oriented to different microgrid aspects, including power electronics, distributed energy-storage systems, hierarchical and cooperative control, energy management systems, smart metering, and the Internet of Things for ac/dc microgrid clusters and islanded minigrids. He specially focused on microgrid technologies applied to offshore wind, maritime microgrids for electrical ships, vessels, ferries and seaports, and space microgrids applied to nanosatellites and spacecrafts.

Dr. Guerrero was elevated as an IEEE Fellow for his contributions to "distributed power systems and microgrids" in 2015. He received the Best Paper Award of the IEEE TRANSACTIONS ON ENERGY CONVERSION for the period 2014–2015, the Best Paper Prize of the IEEE PES in 2015, and the Best Paper Award of the *Journal of Power Electronics* in 2016. During six consecutive years, from 2014 to 2019, he was awarded by Clarivate Analytics (former Thomson Reuters) as a Highly Cited Researcher with 50 highly cited articles. He is an Associate Editor for a number of IEEE TRANSACTIONS.